PHYSICAL REVIEW C VOLUME 59, NUMBER 4 APRIL 1999

Shape coexistence in doubly-magic ^{56}Ni by the Monte Carlo shell model

Takahiro Mizusaki,[1] Takaharu Otsuka,[1,2] Yutaka Utsuno,[1,2] Michio Honma,[3] and Takashi Sebe[4]
[1]*Department of Physics, University of Tokyo, Hongo, Tokyo 113, Japan*
[2]*RIKEN, Hirosawa, Wako-shi, Saitama 351-0198, Japan*
[3]*Center for Mathematical Sciences, University of Aizu, Tsuruga, Ikki-machi Aizu-Wakamatsu, Fukushima 965, Japan*
[4]*College of Engineering, Hosei University, Koganei, Tokyo, 184, Japan*
(Received 28 December 1998)

The structure of low-lying states of ^{56}Ni is studied by the Monte Carlo shell model based on the quantum Monte Carlo diagonalization method. The coexistence of spherical yrast, prolate deformed, and other non-yrast states is described by the full pf-shell calculations, by employing the FPD6 realistic residual interaction. To understand the properties of eigenstates thus obtained, we utilize a mean field analysis, such as a potential energy surface by constrained Hartree-Fock method. [S0556-2813(99)50304-X]

PACS number(s): 21.60.Cs, 27.40.+z

Shape coexistence has been observed in many nuclei. A variety of deformations can coexist in nuclei, e.g., spherical, prolate or oblate deformed, and superdeformed shapes. Recently a clear shape coexistence has been observed [1] in the doubly-magic ^{56}Ni. We shall study, in this Rapid Communication, the shape coexistence in ^{56}Ni within a large-scale shell model by the quantum Monte Carlo diagonalization (QMCD) method [2–5]. We have already applied this method to the study of the yrast states of ^{56}Ni [5]. The yrast level scheme has been demonstrated to be properly described in the full pf-shell calculation with the FPD6 interaction [6], while the validity of the $N=Z=28$ shell closure was examined [5]. In this Rapid Communication, we present a more comprehensive description of the structure of the low-lying states of ^{56}Ni, demonstrating the feasibility of the QMCD calculations for non-yrast states. Moreover, we show that the shell model calculation within a full major shell can produce a distinct spherical-deformed shape coexistence. While such a full major shell calculation has so far been impossible for ^{56}Ni, it has been made possible by the QMCD method. Consequently eigenstates with various types of deformation can be described simultaneously by the same Hamiltonian.

As ^{56}Ni is a self-conjugate nucleus, the coherence between proton-neutron wave functions can get stronger. The effect of the $T=0$ part of the effective interaction can be enhanced, driving the nucleus more deformed. Whether or not a deformation takes place crucially depends on the effective interaction. For instance, if we take too large a $T=0$ strength, the ground state of ^{56}Ni becomes deformed. In an earlier study, we found that the FPD6 interaction [6] is quite reasonable and indeed reproduces the yrast properties of ^{56}Ni [5]. We therefore use the FPD6 interaction throughout this Rapid Communication.

We investigate, in this study, collective excitation modes for low-lying states of ^{56}Ni, in which several nucleons are excited from $f_{7/2}$ into other pf-shell orbits and the nucleus can be strongly deformed. In addition to these collective modes, single particle excitations should be considered. Such modes and their competition can be properly handled in the shell model framework. We thus present a level scheme of ^{56}Ni by a Monte Carlo shell model calculation based on the QMCD method.

Mean field approaches are known to be simple, yet useful, in investigating collective modes of nuclei. It seems that there has been no extensive use of the mean field approach in connection to a spherical shell model. However, a mean field analysis can be incorporated quite nicely into the QMCD calculation, providing us with some insight into the nature of these collective modes. First we consider a constrained Hartree-Fock (CHF) method (see [8,9] for instance) within the given shell model space. Constraints are given for J_x and Q's in a quadratic way:

$$H' = H + \alpha \sum_{\mu} (\langle Q_\mu \rangle - q_\mu)^2 + \beta (\langle J_x \rangle - j_x)^2, \qquad (1)$$

where H, $Q_\mu (\mu = -2, \ldots, 2)$ and J_x are the shell model Hamiltonian, the isoscalar quadrupole operators, and the x-component of the angular momentum operator, respectively, and q_μ's and j_x are parameters. The values of α and β are positive, and are taken so as to achieve convergence of the iteration of the gradient method. We set $j_x = \sqrt{J(J+1)}$ with J being the total angular momentum of the state under consideration. In the following analysis, we take the axially symmetric ansatz: $q_0 = \sqrt{5/(16\pi)}q$ and $q_\mu = 0 (\mu \neq 0)$. Note that q is the intrinsic quadrupole moment. The HF solution to H' in Eq. (1) will be called the CHF state. The potential energy surface (PES) is defined as the expectation value of H with respect to the CHF state for a given q. The PES for ^{56}Ni is shown in Fig. 1(a) as a function of q. Note that the pf-shell model space and the FPD6 interaction are used. In Fig. 1(b), the occupation numbers of the $f_{7/2}$ orbit are shown.

In Fig. 1(a), the first minimum appears at $q \sim 0$ for low-spin states. In the ground state, this minimum corresponds to the $(f_{7/2})^{16}$ configuration, i.e., the doubly-magic shell. On the other hand, a pronounced deformed minimum shows up at $q \sim 85\ e\ \mathrm{fm}^2$ for each spin. These deformed minima are referred to as prolate minima hereafter. As we shall see, a prolate band is constructed upon this minimum. The barrier between two minima is as high as 5 MeV for the 0^+ state, and it decreases gradually as the spin goes up. These double minima are a characteristic feature of shape coexistence. The occupation number of the $f_{7/2}$ orbit for the prolate minimum is about 10.5 as shown in Fig. 1(b). This value is rather constant for each spin.

 ©1999 The American Physical Society

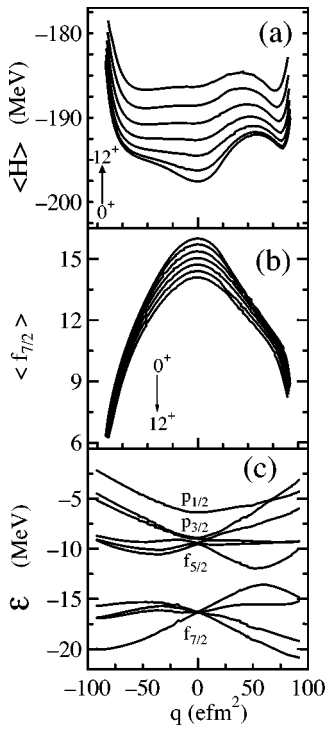

FIG. 1. (a) Potential energy surface in CHF; (b) occupation numbers of $f_{7/2}$ orbit; (c) deformed single particle energies, as functions of q.

The CHF states are, in general, neither eigenstates of the shell model Hamiltonian nor of angular momentum. While CHF can give some guidance concerning the nature of certain states, the full wave function will contain many more configurations, and therefore a full diagonalization is required. To obtain the eigenstates, we proceed to the QMCD shell model calculation.

In this method, as candidates for basis vectors for diagonalization of the shell model Hamiltonian, Slater determinants are stochastically generated by starting from the mean-field solution [4]. These Slater determinants have the following form [4]: $e^{-\beta(h_{MF}+\sigma_\alpha O_\alpha)}|\Psi\rangle$, where $h_{\rm MF}$ is a mean field one-body Hamiltonian; the O's express one-body fields and the σ's are taken randomly [2]. The generated bases are selected from these candidates by referring to the energy eigenvalue obtained by the diagonalization. Note that this energy eigenvalue can be the one for an excited state when bases are sampled for the corresponding eigenstate. This basis-sampling process is actually done for the magnetic quantum number (M-) projected [3] or total angular momentum (J-) projected [5] Slater determinant. The former (latter) is called $M(J)$-*compression* [5]. A calculation by the latest method (i.e., phase III) is presented for yrast states in [5].

In obtaining non-yrast eigenstates, there are, in general, two aspects. One is the proper basis-sampling for considering dynamics, while the other is an orthogonalization condition to other eigenstates with the same quantum numbers during the basis-sampling process. The latter can be, in general, properly handled in the *J-compression* calculation because each basis state has a definite angular momentum due to the angular momentum projection and the diagonalization ensures the orthogonality among eigenstates.

In the case of the prolate band of ^{56}Ni, the basis generation is simpler because the eigenstates are formed predominantly by states related to the deformed local minimum. We therefore calculate such eigenstates by performing the basis-sampling around the second minimum. This is simply achieved by substituting the CHF one-body Hamiltonian at $q=60\sim90\ e\ \mathrm{fm}^2$ to $h_{\rm MF}$. The orthogonality to the yrast state is fulfilled to a large extent because of the large difference of deformation. Moreover, during the *J-compression* basis-sampling, the orthogonality condition between the yrast and the prolate states is explicitly taken into account by the diagonalization procedure.

Except for the spherical and prolate minima, there is no other definite minimum in Fig. 1(a) and it is difficult to foresee other eigenstates without the diagonalization of the shell model Hamiltonian. In order to obtain a non-yrast state, we carry out the *J-compression* calculation as discussed below. The number of the basis-sampling steps depends on the choice of $h_{\rm MF}$ for a considered state. For yrast states, a one-body Hamiltonian of the HF [4] or cranked HF [5] is used for $h_{\rm MF}$. For the state formed in a rather isolated minima, the one-body Hamiltonian of the constrained HF is utilized, as discussed above. For the general case, the structure of the J-projected energy surface can be useful. For instance, as we will discuss later, the generator coordinate method (GCM) [8,9] calculation for the shell model can approximately give energy levels, including non-yrast states. The GCM eigenstates are obtained by diagonalizing the Hamiltonian by using CHF states as the bases with constraints for appropriately chosen ''coordinates.'' These coordinates span a GCM parameter space. In this space, we can find a region relevant to the eigenstate being calculated. This is the region where the QMCD basis sampling is started and also is carried out primarily. The $h_{\rm MF}$'s of this region are determined by the CHF method for the corresponding q values. In the GCM, a parameter space is spanned by few variables, while in the QMCD basis sampling, this restriction is absent. Hence, after the sufficient QMCD basis-sampling, QMCD eigenstates can become quite different from the GCM eigenstates by incorporating various correlations outside the GCM. In this way, we can obtain precise wave functions, properly considering the two aspects above.

In Fig. 2, the obtained energy spectra and the $B(E2)$ values are shown, where 45 bases are taken in total for each spin. Only the large $B(E2)$'s are indicated. The effective charges $e_\pi=1.23e$ and $e_\nu=0.54e$ are taken [5] which is similar to other choices in this region; see for comparison [1,6,7].

As we already reported in Ref. [5], the experimental level scheme is well reproduced for yrast states by the present calculations. A salient feature of ^{56}Ni is the appearance of the excited rotational band. The QMCD calculation indeed reproduces the experimental levels of this rotational band, as seen in Fig. 1. This is nothing but the prolate band in CHF. The bandhead energy calculated by the QMCD is 4.6 MeV. The rotational states are formed on top of this 0_p^+ state in Fig. 2. The subscript p denotes the members of this prolate band hereafter. The sum of the $B(E2)$'s from the 0_p^+ state is 2334 e^2 fm^4, which is about three time larger than the one for the 0_1^+ state [5]. This shows a large collectivity of the prolate states.

We consider the quadrupole moments and inband $E2$

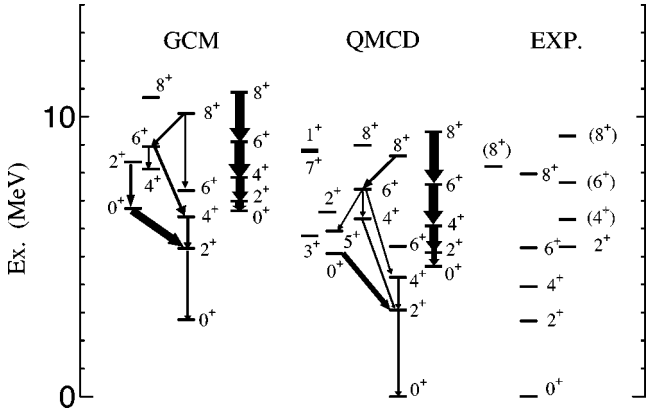

FIG. 2. Experimental levels [1,12] of ^{56}Ni compared with QMCD and GCM results with a FPD6 Hamiltonian. The GCM energies are shown relative to the QMCD ground state. The $B(E2{:}(J+1 \text{ or } 2)\rightarrow J^+)$ values, which are larger than 100 e^2 fm^4, are indicated by the width of the arrows.

strengths. The intrinsic quadrupole moment q is about 85 e fm^2 for the local minimum in Fig. 1(a). Assuming $K=0$, the spectroscopic quadrupole moments are estimated as $Q=-J/(2J+3)(q/e)(e_\pi+e_\nu)$, which turn out to be -43, -55, -60, and -63 e fm^2 for 2_p^+, 4_p^+, 6_p^+, and 8_p^+, respectively. These are consistent with those computed from QMCD eigenstates: -43, -54, -61, and -65 e fm^2, respectively. In the same way, we can estimate the inband $E2$ strengths by $B(E2{:}J^+\rightarrow(J+2)^+)_{\rm MF}=(5/16\pi)(e_\pi+e_\nu)^2(q/e)^2|\langle J020|J+2,0\rangle|^2$, which take the values, 2251, 1157, 1023, and 970 e^2 fm^4, for $J=0,2,4,6$, respectively. On the other hand, in the QMCD calculation, the same $B(E2)$'s are 1865, 1118, 904, and 834 e^2 fm^4, respectively. Sizable differences exist, while the mean field values give a good approximation. The deformation parameter β_2 [10] evaluated from these $B(E2)$'s is about 0.32. This value appears to be large for the pf-shell and heavier nuclei, indicating a strong deformation. We comment that the intrinsic quadrupole moment has been studied by HF+SLy4 and truncated shell model calculations in Ref. [1].

The magnetic moments of the yrast (prolate) QMCD states are 1.01(1.01), 2.03(2.02), 3.02(3.03), and 4.04(4.05) (μ_N^2) for 2^+, 4^+, 6^+ and 8^+ states, respectively, where we use the spin g factor quenched by a factor of 0.8.

The mean-field description gives us a rather good picture of the prolate band. However, the projected energy of the intrinsic state is still about 2 MeV higher than the one obtained by the QMCD calculation. The QMCD calculation gathers many correlated bases, and the mixing between yrast and prolate states is also included. Consequently a considerable energy shift is obtained and the wave function is improved. To clarify this point, we compute the overlap between the wave function projected from the CHF state at the local minimum and the corresponding QMCD eigenstate. The overlap probabilities are 0.45, 0.54, 0.46, 0.52, and 0.53 for 0_p^+, 2_p^+, 4_p^+, 6_p^+ and 8_p^+, respectively. Mean field components in the QMCD wave functions are about half.

Next we consider the occupation numbers of each orbit in the QMCD wave functions. The occupation numbers of $f_{7/2}$ for the 0_1^+, 2_1^+, 4_1^+, 6_1^+, and 8_1^+ states are 14.6, 13.0, 13.2, 13.6, and 13.4, respectively. On the other hand, the corresponding numbers for the prolate states are 10.9, 10.6, 10.6, 10.5, and 10.5, respectively, and are rather constant. These values are also consistent with the CHF value in Fig. 1(b). Thus, the prolate deformed band is mainly generated by exciting four nucleons to upper pf-shell orbits from the ground state.

The conventional shell model diagonalization in the truncated model space is also carried out, allowing up to $6p6h$ excitations from $f_{7/2}$ to upper orbits. This calculation is one of the state-of-the-art calculations with dimension reaching 24.7 million in the M scheme. For the 0_1^+ and 2_1^+ states, the results were reported in Ref. [5]. The QMCD results are better than those of this shell model calculation, especially, in the 2_1^+ level [5].

Here we make a similar comparison for prolate deformed states. Since the CHF result indicates that the average particle-hole excitation is about $6p6h$, this $6p6h$ truncation may not be rational. However the $6p6h$ truncated shell model calculation can produce the precursor of the prolate band as intruder states. The bandhead energy appears about 1.6 MeV higher than the QMCD calculation. The average number of excited nucleons is 3.5 for this 0^+ state of the $6p6h$ shell model, while it reaches 5.1 for the QMCD. Concerning the inband $B(E2{:}0^+\rightarrow 2^+)$, the $6p6h$ value is smaller by a factor of 3 than the QMCD value. At the $6p6h$ truncation, the prolate band structure keeps developing gradually as the shell model space becomes larger.

In addition to the prolate states, we investigate other non-yrast levels. There are few experimental levels [1], while the FPD6 interaction predicts several non-yrast states at low energy. For these states, the PES does not help so much because the PES at $q<0$ is rather flat. The QMCD method can still describe these states without much difficulty, as shown below. For instance, a third 0^+ state exists near the second 0^+ state. The sum of $E2$ strengths from the 0_3^+ state is 1660 e^2 fm^4, i.e., about twice larger than the one for the 0_1^+ state. Thus, the 0_3^+ state is rather collective. Some other levels are shown in Fig. 2.

In order to understand the origin of these states, we go back to the GCM calculation for the ''coordinate'' q. The q axis is divided into 45 mesh points, and the Hamiltonian is diagonalized for the J-projected bases on these mesh points. As the realistic shell model has various degrees of freedom, it is, in general, difficult to specify the shell model eigenstate only by one parameter q. Consequently the obtained eigenenergies are rather poor compared to those of the QMCD method: for instance, 2.7 MeV too high for 0_1^+. The same GCM calculations are done for other spins and the results are shown in Fig. 2. For other spins, eigenvalues are also 2 $\sim$2.5 MeV higher than those of the QMCD calculations. Consequently the GCM calculations can give a qualitatively similar level scheme to the QMCD results. For the prolate states, the quadrupole moments and the $B(E2)$'s of the GCM eigenstates are similar to those of the QMCD eigenstates, except for the $0_p^+\rightarrow 2_p^+$ transition. The $B(E2)$'s of the GCM calculations are 2514, 1049, 1081 and 865 e^2 fm^4 for $0_p^+\rightarrow 2_p^+$, $2_p^+\rightarrow 4_p^+$, $4_p^+\rightarrow 6_p^+$, and $6_p^+\rightarrow 8_p^+$, respectively. On the other hand, for other states, the $B(E2)$'s are quantitatively rather different, as shown in Fig. 2.

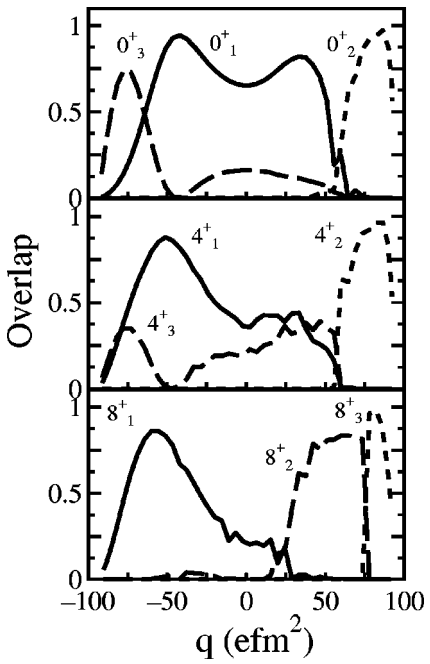

FIG. 3. Overlaps between the J-projected CHF state and GCM eigenfunctions for 0^+, 4^+, and 8^+ states.

Although the eigenenergies of the GCM are not so accurate, the GCM can give us an improved understanding about the shell model, compared to the CHF. For instance, a GCM eigenstate can be directly related to mean field by the overlap with a CHF state of a given value of q. In Fig. 3, this overlap is shown for 0^+, 4^+, and 8^+ states as functions of q. We confirm that the prolate states originate sharply in the prolate region. Moreover the 0^+_3, 2^+_3, 4^+_3, and 6^+_2 states are found to be excited states with nodal structure in the wide oblate well. Note that this seems to be a first attempt to apply the GCM to shell model calculations. The present GCM calculations are carried out under the axially symmetric ansatz. In a forthcoming paper, this restriction will be lifted.

In Fig. 2, one state is experimentally known near the 8^+_1, whose spin has not been assigned. In the QMCD level scheme, a candidate of this state is 8^+_2. This state is interesting because in the QMCD calculation its quadrupole moment is 62 e fm^2 and the occupation number of $f_{7/2}$ is 12.8. The difference of the occupation number of $f_{7/2}$ between the ground state and this 8^+_2 state is $14.6-12.8=1.8$, which suggests the $2p2h$ excitation from the correlated ground state as the main component of this state. By the GCM analysis, this state is composed of the bases at $q=25\sim75$ e fm^2 as shown in Fig. 3. To understand the origin of this state, we examine the CHF deformed single particle energies as shown in Fig. 1(c). This diagram is somewhat similar to Nilsson's diagram [11]. In the FPD6 interaction, the spherical single particle energies with respect to the ^{40}Ca core are taken as -8.39, -6.50, -1.90, and -4.48 MeV for $f_{7/2}$, $p_{3/2}$, $f_{5/2}$, and $p_{1/2}$, respectively. In the diagram of Fig. 1(c), on the other side, the $f_{5/2}$ and $p_{3/2}$ are almost degenerate at $q=0$ for ^{56}Ni. At $q<0$, a $N=Z=28$ shell gap remains prominent, while at $q>0$, orbits from the upper shell come down. For ^{56}Ni, the fifth deformed orbit is relevant to the present point. This orbit is mainly an admixture of $f_{5/2}$ and $p_{3/2}$. At $q>50$ e fm^2, the upper orbits are considerably admixed with $f_{7/2}$. The resultant CHF state has large components of upper orbits and becomes deformed. Thus the prolate band appears.

For $q>20$ e fm^2, as the fifth orbit comes down, the excitation across the Fermi surface can easily take place. To generate a higher spin state, this excitation is energetically favored around the crossing of the fourth and fifth orbits. We expect that the 8^+_2 state is predominantly a CHF state of this nature. We confirm this in two ways. The K quantum numbers of these orbits before the crossing are 7/2 and 1/2, respectively. If two nucleons jump across the Fermi surface, the total K becomes $2\times(7/2\pm1/2)=6$ or 8. We assume $K=8$. The spectroscopic quadrupole moment can be estimated from the mean field value as $Q=\frac{40}{57}(q/e)(e_\pi+e_\nu)\sim62$ e fm^2, for $q\sim50$ e fm^2. This estimate agrees with the quadrupole moment of the QMCD wave function. Moreover the angular momentum projection from the CHF state at $q\sim50$ e fm^2 produces a wave function with a quadrupole moment as large as that of the 8^+_2 state.

For the lower spin states, the '$1p1h$' excitation is enough for spin coupling, because the '$1p1h$' excitation from $f_{7/2}$ to $f_{5/2}$ brings about the angular momentum $1^+\sim6^+$, while the '$2p2h$' excitation $2^+\sim12^+$. Here, ' ' means excitation from the ground state to upper orbits. The former is energetically favored for low-spin states. In the QMCD eigenstates, the occupation numbers of $f_{7/2}$ for $0^+_1\sim7^+_1$ and 8^+_2 states are 14.6, 13.7, 13.0, 13.4, 13.2, 13.5, 13.6, 12.4, and 12.8, respectively. Thus, the $1^+_1\sim6^+_1$ states are of '$1p1h$' excitation nature.

In summary, we demonstrated the feasibility of QMCD calculations for non-yrast states. For obtaining such states, we extended the QMCD method, considering the underlying dynamics. We utilized the CHF method and GCM as a guide for the basis-sampling of the QMCD calculation. Consequently we were able to obtain the yrast, prolate, and oblate states of ^{56}Ni. To understand the obtained wave functions, we performed a mean field analysis with the shell model Hamiltonian and space. By the CHF analysis, we found the existence of the prolate deformed band. In general the CHF analysis can play an indispensable role in clarifying the basic structure of the collective modes embedded in a shell model space. For instance, we found the deformed minima for the semimagic nuclei in the pf-shell region such as ^{54}Fe [13]. Moreover, we predicted other low-lying non-yrast states. By introducing the GCM calculations and the single particle energy diagram, the origin of these states can be suggested as being a collective excitation mode in the oblate well and single-particle excitation mode.

Recent experimental data [1] show that ^{56}Ni has two deformed side bands. In this study, we pointed out that the lower deformed band can be understood within the pf-shell calculation. For the description of the other deformed band, the explicit $g_{9/2}$ degree of freedom seems to be essential. We are pursuing this interesting problem by the same method, extending the shell model space.

We acknowledge Professor P. von Brentano and Professor A. P. Zuker for fruitful discussions. We are grateful to Professor A. Gelberg for reading the manuscript. This work was supported in part by Grant-in-Aid for Scientific Research (B) (No. 08454058) and (A)(2)(10304019) from the Ministry of Education, Science and Culture.

[1] D. Rudolf *et al.*, Phys. Rev. Lett. (submitted).
[2] M. Honma, T. Mizusaki, and T. Otsuka, Phys. Rev. Lett. **75**, 1284 (1995).
[3] T. Mizusaki, M. Honma, and T. Otsuka, Phys. Rev. C **53**, 2786 (1996).
[4] M. Honma, T. Mizusaki, and T. Otsuka, Phys. Rev. Lett. **77**, 3315 (1996).
[5] T. Otsuka, M. Honma, and T. Mizusaki, Phys. Rev. Lett. **81**, 1588 (1998).
[6] W.A. Richter, M.G. van der Merwe, R.E. Julies, and B.A. Brown, Nucl. Phys. **A523**, 325 (1991).
[7] G. Kraus *et al.*, Phys. Rev. Lett. **73**, 1773 (1994).
[8] P.-H. Heenen *et al.*, in *Proceedings of the International Workshop ''Nuclear Structure Models,''* Oak Ridge, Tennessee, 1992, edited by R. Bengtsson, J. Draayer, and W. Nazarewicz (World Scientific, Singapore, 1993), p. 3.
[9] P. Ring and P. Schuck, *The Nuclear Many-Body Problem* (Springer-Verlag, New York, Heidelberg, Berlin, 1980).
[10] S. Raman *et al.*, At. Data Nucl. Data Tables **36**, 1 (1987).
[11] For instance, A. Bohr and B. R. Mottelson, *Nuclear Structure* (Benjamin, New York, 1969), Vol. 1.
[12] *Table of Isotopes*, edited by R. B. Firestone *et al.* (Wiley, New York, 1996).
[13] D. Rudolf *et al.*, Nucl. Phys. **A630**, 417c (1998).